

Quantitative analysis of WC stars: Constraints on neon abundances from ISO/SWS spectroscopy

Luc Dessart^{1*}, Paul A. Crowther¹, D. John Hillier², Allan J. Willis¹,
Patrick W. Morris^{3,4†}, Karel A. van der Hucht⁴

¹: Dept. of Physics & Astronomy, University College London, Gower St., London, UK.

²: Dept. of Physics & Astronomy, University of Pittsburgh, PA 15260, USA.

³: Astronomical Institute “Anton Pannekoek”, University of Amsterdam, NL-1098 SJ Amsterdam, the Netherlands

⁴: Space Research Organization Netherlands, Sorbonnelaan 2, NL-3584 CA Utrecht, the Netherlands

Accepted/Received

ABSTRACT

Neon abundances are derived in four Galactic WC stars – γ^2 Vel (WR11, WC8+O7.5III), HD 156385 (WR90, WC7), HD 192103 (WR135, WC8), and WR146 (WC5+O8) – using mid-infrared fine structure lines obtained with ISO/SWS. Stellar parameters for each star are derived using a non-LTE model atmospheric code (Hillier & Miller 1998) together with ultraviolet (IUE), optical (INT, AAT) and infrared (UKIRT, ISO) spectroscopy. In the case of γ^2 Vel, we adopt results from De Marco et al. (2000), who followed an identical approach.

ISO/SWS datasets reveal the [Ne III] $15.5\mu\text{m}$ line in each of our targets, while [Ne II] $12.8\mu\text{m}$, [S IV] $10.5\mu\text{m}$ and [S III] $18.7\mu\text{m}$ are observed solely in γ^2 Vel. Using a method updated from Barlow et al. (1988) to account for clumped winds, we derive $\text{Ne/He}=3\text{--}4\times 10^{-3}$ by number, plus $\text{S/He}=6\times 10^{-5}$ for γ^2 Vel. Neon is highly enriched, such that Ne/S in γ^2 Vel is eight times higher than cosmic values. However, observed Ne/He ratios are a factor of two times lower than predictions of current evolutionary models of massive stars. An imprecise mass-loss and distance were responsible for the much greater discrepancy in neon content identified by Barlow et al.

Our sample of WC5–8 stars span a narrow range in T_* ($=55\text{--}71\text{kK}$), with no trend towards higher temperature at earlier spectral type, supporting earlier results for a larger sample by Koesterke & Hamann (1995). Stellar luminosities range from $100,000$ to $500,000L_\odot$, while $10^{-5.1} \leq \dot{M}/(M_\odot\text{yr}^{-1}) \leq 10^{-4.5}$, adopting clumped winds, in which volume filling factors are 10%. In all cases, wind performance numbers are less than 10, significantly lower than recent estimates. Carbon abundances span $0.08 \leq \text{C/He} \leq 0.25$ by number, while oxygen abundances remain poorly constrained.

Key words: stars: Wolf-Rayet – infrared – abundances – evolution – individual: WR11, WR90, WR135, WR146

1 INTRODUCTION

Understanding the physics of massive ($M_{\text{init}} \gtrsim 25 M_\odot$) stars, their atmospheres, radiation, and evolution is important for many aspects of astrophysics since their powerful winds affect the energy and momentum balance of the interstellar

medium (ISM). In particular, Wolf-Rayet (WR) stars provide crucial tests of nuclear reaction chains.

However, quantitative analysis of such stars, represents a formidable challenge. The assumptions of plane-parallel geometry and local thermodynamic equilibrium (LTE), which are often adopted for lower luminosity stars, are inadequate. Nevertheless, the properties of a large sample of carbon sequence (WC-type) WR stars have now been quantitatively derived using detailed models, accounting for non-LTE effects, spherical geometry and an expanding atmosphere (Howarth & Schmutz 1992; Koesterke & Hamann 1995). However, recent studies have demonstrated that clumping (Moffat et al. 1988; Hillier 1991, 1996;

* Present Address: Département de Physique, Université Laval and Observatoire du Mont Mégantic, Québec, QC G1K 7P4, Canada; email: ldessart@orion.phy.ulaval.ca

† Present Address: SIRTf Science Center/IPAC, California Institute of Technology, M/S 100-22, 1200 E. California Blvd, Pasadena, CA 91125, USA

Schmutz 1997) and line blanketing (Schmutz 1997; Hillier & Miller 1998) may have a significant effect on the derived physical properties of WR stars.

Overall, evolutionary predictions for massive stars (e.g. Meynet et al. 1994) are in good agreement with the observed properties of Wolf-Rayet stars. van der Hucht & Olon (1985) derived a Ne/He ratio for γ^2 Vel (WR11, HD 68273, WC8+O7.5) from IRAS space-based observations, which was found to be in good agreement with expectations. However, Barlow et al. (1988, hereafter BRA88) identified a numerical flaw in these calculations and added new ground-based observations to reveal Ne/He=1.0±0.35×10⁻³, a factor of six lower than predicted. Is this discrepancy due to failure of evolutionary models, peculiarities of the γ^2 Vel binary system, or incorrect assumptions for the stellar properties of the WC8 star? The combination of Short Wavelength Spectrometer (SWS), Infrared Space Observatory (ISO) observations of a larger sample of WC stars, plus recent progress in quantitative modelling of WR stars, should provide a definitive answer to this question.

Recent space-based spectroscopy of WR11, obtained with the Infrared Space Observatory (ISO), was presented by van der Hucht et al. (1996). who quoted excellent agreement of the fine-structure neon line fluxes with observations used by BRA88. Morris et al. (1998) subsequently re-estimated Ne/He using contemporary information on the stellar distance (van der Hucht et al. 1997; Schaerer et al. 1997) and mass-loss rate (Stevens et al. 1996) of WR11, which revealed a considerable neon enrichment. Willis et al. (1997, hereafter Paper I) also used ISO/SWS to observe WR146, another WC+O binary, again revealing significantly enriched neon. Recently, Morris et al. (2000) analysed ISO/SWS observations of WR147 (WN8+OB), revealing neon, sulphur and calcium abundances in good agreement with cosmic values, as expected by evolutionary models.

In this paper, we supplement results from Paper I with other WC stars for which ISO-SWS observations are available, HD 156385 (WR 90, WC7) and HD 192103 (WR135, WC8). We also re-analyse WR146 (WC5+O8) using more sophisticated analysis techniques and in the light of other observational evidence (Niemela et al. 1998; Dougherty et al. 2000). A neon abundance is also re-derived for WR11, following recent spectroscopic results from De Marco et al. (2000).

The outline of the present work is as follows. New UV, optical and IR observations of our programme stars are presented in Sect. 2, with basic properties discussed in Sect. 3. The spectroscopic technique is introduced in Sect. 4, and applied in Sect. 5. Our spectroscopic results are discussed in Sect. 6, with neon and sulphur abundances derived in Sect. 7. Finally, conclusions are reached in Sect. 8.

2 OBSERVATIONS

The programme Galactic WC stars are listed in Table 1 where we give the various catalogue names and our adopted spectral types, following Smith et al. (1990) and Crowther et al. (1998). We will refer to our programme stars by their WR catalogue number (van der Hucht et al. 1981). Wind velocities are taken from UV resonance line measurements (Prinja

Table 1. Programme Galactic WC stars. Spectral types are obtained from Crowther et al (1998), which follows Smith et al. (1990) except that revised WCE criteria are adopted. Wind velocities are taken from (a) Prinja et al. (1990), (b) Willis et al. (1997), or (c) St Louis et al. (1993)

| WR | HD | Other | v_∞ km s ⁻¹ | Ref. | Spectral Type |
|-----|--------|----------------|----------------------------------|------|------------------|
| 11 | 68273 | γ^2 Vel | 1550 | c | WC8+O7.5III |
| 90 | 156385 | | 2045 | a | WC7 |
| 135 | 192103 | V1042 Cyg | 1405 | a | WC8 |
| 146 | | HM19-3 | 2700 | b | WC5+O8 |

Table 2. Journal of optical and IR spectroscopic observations. All SWS observations were obtained with the AOT06 scan.

| WR | Epoch | Telescope Inst. | Wavelength Range (μ m) | Exposure Time (s) |
|-----|----------------|--------------------|--------------------------------|----------------------|
| 11 | 17 May 1996 | ISO-SWS | 2.38–45.2 | 7,876 |
| 90 | 9 Mar 1998 | AAT-RGO | 0.50–1.03 | 5 |
| | 16 Feb 1997 | ISO-SWS | 2.60–19.6 | 10,068 |
| 135 | Sep 1991 | INT-IDS | 0.38–0.73 | 24 |
| | 20 Aug 1994 | UKIRT-CGS4 | 1.03–1.13 | 64 |
| | 19–21 Aug 1994 | UKIRT-CGS4 | 1.61–2.21 | 576 |
| | 21 Aug 1994 | UKIRT-CGS4 | 2.30–2.51 | 128 |
| | 11 Nov 1996 | ISO-SWS | 2.38–45.2 | 6,538 |
| 146 | 21 Jul 1996 | INT-IDS | 0.36–0.68 | 800 |
| | 19 Aug 1994 | UKIRT-CGS4 | 1.03–1.13 | 64 |
| | 20 Aug 1994 | UKIRT-CGS4 | 1.23–1.33 | 64 |
| | 19–21 Aug 1994 | UKIRT-CGS4 | 1.61–2.21 | 224 |
| | 21 Aug 1994 | UKIRT-CGS4 | 2.30–2.51 | 64 |
| | 12 May 1996 | ISO-SWS | 2.60–19.6 | 16,922 |

et al. 1990; St Louis et al. 1993), except for WR146 for which a terminal velocity was obtained in Paper I from ISO/SWS spectroscopy. In this section, we discuss the ground-based (AAT, INT, ESO) and space-based (ISO, IUE) observations, the journal of which is presented in Table 2.

2.1 Ultraviolet spectroscopy

Our UV dataset was obtained solely from the International Ultraviolet Explorer (IUE) archive. Available high dispersion (HIRES), large aperture, short-(SWP) and long-wavelength (LWP, LWR) observations of WR90 and WR135 were combined to provide high S/N datasets (St Louis 1990). Absolute flux calibration was achieved following the calibration curve obtained by Howarth & Phillips (1986). Agreement between our final HIRES datasets and archival low resolution (LORES) observations was found to be excellent.

Willis et al. (1986) have discussed the UV spectral morphology of WC stars, including WR90 and WR135. The principal spectral features for both stars are Si IV $\lambda\lambda$ 1393–1407, C IV $\lambda\lambda$ 1548–51, He II λ 1640, and C III λ 2297. A forest of Fe V–VI lines are present in both stars, with Fe IV also prominent in WR135.

2.2 Optical spectroscopy

Previously unpublished spectroscopic observations of WR90 and WR135 were obtained at the 2.5m Isaac Newton Tele-

scope (INT) and 3.9m Anglo Australian Telescope (AAT). The INT dataset was obtained with the IDS, 500mm camera, and GEC CCD during 1991 September, while the AAT dataset was obtained with the RGO spectrograph, 25cm camera, and a MIT/LL CCD during 1998 March. Each dataset was obtained using CCDs and reduced in a standard manner using software available on STARLINK. Spectra were debiased, flat-fielded, optimally extracted, wavelength calibrated, and flux calibrated in the case of the INT dataset. Flux calibration was achieved for the AAT observations via scaling to the level of the blue CTIO spectrophotometry taken from Torres-Dodgen & Massey (1988).

Arc spectra provided a measure of the instrumental resolution: 2–3Å (INT) and 4Å (AAT). Complete spectral coverage between 3800–7300Å (INT) and 5000–10300Å (AAT) was achieved with, respectively, six and one grating settings. The atmospheric absorption bands removed using suitable comparison stars.

The optical spectral appearance of WR146 has previously been discussed in Paper I, while Dougherty et al. (2000) present a new high quality blue optical observation of that star. The morphologies of WR90 and WR135 are relatively similar, dominated by He I-II and C III-IV emission features, except that the emission lines of WR90 are substantially broader. C III $\lambda\lambda$ 4747–51 and C IV $\lambda\lambda$ 5801–12 are the two strongest features in each case. Several O III-V features are present around $\lambda\lambda$ 2950–3150, and λ 5592 with C II present at λ 4267 for WR135.

2.3 Near-IR spectroscopy

Our principal near-IR dataset was obtained at the 3.8m U.K. Infrared Telescope (UKIRT) with the cooled grating spectrograph CGS4, the 300mm camera, a 751/mm grating and a 62×58 InSb array in 1994 August. Observations of WR135 and WR146 were bias-corrected, flat-fielded, extracted and sky-subtracted using CGS4DR (Daly & Beard 1992). Subsequent reductions and analysis were carried out using FIGARO (Shortridge et al. 1999) and DIPSO (Howarth et al. 1998). In order to remove atmospheric features, the observations were divided by an appropriate standard star (whose spectral features were artificially removed) observed at around the same time and similar air mass. In regions of low atmospheric transmission at UKIRT the reliability of line shape and strength must be treated with caution (e.g. the P α region). The near-IR morphology of WR135 and WR146 have been discussed previously by Eenens, Williams & Wade (1991).

We also utilise intermediate dispersion CCD spectra of WR135 covering 0.97–1.03 μ m, published by Howarth & Schmutz (1992), and obtained at the INT with the Intermediate Dispersion Spectrograph (IDS) and a GEC CCD in 1990 October. Although Howarth & Schmutz (1992) obtained observations of the He I λ 10830+P γ line, we prefer to use our new, lower resolution UKIRT observations of this feature. (The sharp fall in efficiency of the GEC CCD longward of P γ leads to an ill-defined continuum.). We attempt an approximate flux calibration for these data, by setting the local continuum via interpolation of the observed 0.7 μ m (INT) and 1.03 μ m (UKIRT) flux levels.

Table 3. Summary of photometry, reddenings and distances for programme stars, including comparisons with reddenings from the literature (lit). Observed magnitudes correspond to the systemic value for binary systems, and include the Schmutz & Vacca (1991) corrections to Smith (1968) photometry (*)

| WR | v^{sys} mag | Ref. | E_{B-V} (lit) mag | R | Ref. | M_v^{WC} mag | d kpc | Ref |
|-----|-------------------------|------|------------------------|-----|------|--------------------------|------------|-----|
| 11 | 1.70* | a | 0.04 (0.03) | 3.1 | e | −3.7 | 0.26 | h |
| 90 | 7.41* | a | 0.38 (0.44) | 3.1 | d | −4.7 | 1.55 | e |
| 135 | 8.51 | b | 0.37 (0.35) | 3.1 | a | −4.3 | 2.09 | f |
| 146 | 13.91 | c | 2.87 (2.80) | 2.9 | c | −5.3 | 1.40 | g |

a: Smith (1968), b: Massey (1984), c: Paper I, d: Morris et al. (1993) e: Schaerer et al. (1998), f: Lundström & Stenholm (1984), g: Dougherty et al. (2000), h: van der Hucht et al. (1997)

2.4 Mid-IR spectroscopy

New mid-IR data of WR90 and WR146 were obtained as part of Guest Observer programme, AJWWOLF (P.I. Willis), with the Short Wavelength Spectrograph (SWS; de Graauw et al. 1996) onboard the ESA Infrared Space Observatory (Kessler et al. 1996). Observations of HD 117297 (WR53), HD 164270 (WR103) and HD 165763 (WR111) from the AJWWOLF programme were of insufficient quality to provide mid-IR line flux measurements, and so these were excluded from the present study. Consequently, we have included SWS observations of WR11 and WR135 from the Guaranteed Time programme WRSTARS (P.I. van der Hucht). In all cases the SWS AOT6 observing mode was used to achieve full grating resolution, $\lambda/\Delta\lambda \sim 1300 - 2500$. The continuous wavelength coverage was 2.60–19.6 μ m for datasets from the AJWWOLF programme, and 2.38–45.0 μ m for WR135 and WR11.

Data of detector “bands” 1 and 2 respectively cover wavelengths of 2.38–4.08 μ m using 12 In:Sb detectors and 4.00–12.05 μ m with 12 Si:Ga detectors, employing entrance slits that give an effective aperture area of 14 × 20 arcsec on the sky. Band 3A to 3D data cover 12.0–27.6 μ m using 12 Si:As detectors, with sky coverage of 14 × 27 arcsec. finally, band 3E and 4 data cover 27.5–45.0 μ m using 12 Ge:Be detectors, with sky coverage of 20×33 arcsec.

The total integration time was set to allow one complete scan over the wavelengths selected within each “AOT band”, defined by the permissible combinations of detector band, aperture, and spectral order (cf. de Graauw et al. 1996). The observation time includes dark current measurements, and a monitor of photometric drift for the detectors of bands 2–3. A drift measurement is not normally made for the relatively stable In:Sb detectors.

The data processing of the SWS data for WR146 was discussed in Paper I, with WR11, WR90 and WR135 reduced in a similar manner. The stellar spectrum of WR11 will be discussed elsewhere (Morris et al. 2000, in prep), with solely mid-IR fine structure line fluxes measured here.

3 INTERSTELLAR REDDENING AND DISTANCES

In this section, interstellar reddenings and distances to the programme stars are discussed. Pre-empting results from Sect. 4, reddenings are directly obtained from comparing theoretical synthetic spectra with de-reddened observations. Distances either follow from cluster/association membership, or assumed absolute magnitudes. Table 3 provides a summary of the derived reddenings and distances for our sample of stars. A comparison with reddenings from the recent literature shows good agreement. The distances to WR135 (Cyg OB3 member) and WR11 (HIPPARCOS) are known with confidence, while those adopted here for WR90 and WR146 deserve comment.

3.1 WR 90

WR90 is not a member of an association or cluster. We therefore estimated its distance based on the mean absolute visual magnitude of other Galactic WC7 stars. Unfortunately, all five WC7 stars that are members of associations/clusters are within binary systems (Lundstrom & Stenholm 1984). We restricted the sample to those for which reliable reddenings were known (HD97152=WR42, HD152270=WR79 and HD192641=WR 137) from Morris et al. (1993). An absolute visual magnitude of $M_v = -4.7$ mag ($\sigma=0.8$) was obtained for the WC7 components by comparing their emission line strengths with WR90 (specifically C III-IV λ 4650, C IV λ 5804). Our estimate is in good agreement with van der Hucht et al. (1988) and Smith et al. (1990) who derived $M_v = -4.8$ mag. Pre-empting results from Sect. 5 we derive $E_{B-V}=0.38$ mag, so that the uncertainty in the calibration and reddening (± 0.02 mag) implies $d=1.55 \text{ kpc}_{-0.4}^{+0.5}$.

3.2 WR 146

Dougherty et al. (1996) used IR and mm photometry to estimate a distance of 1.2 ± 0.3 kpc towards WR146. Radio observations revealed two separate components, namely the (thermal) WC emission plus the (non-thermal) bow shock emission between the two winds.

Meanwhile, a lower distance of 0.75 ± 0.15 kpc was derived in Paper I, using the mean M_v for a WCE star (Smith et al. 1990), plus an assumed spectral type of O8.5 V for the companion. Subsequently, Niemela et al. (1998) used WFPC2 aboard the Hubble Space Telescope (HST) to measure the individual UVB magnitudes of the WC and OB components of WR146. They derived $V=13.64$ mag for the WC star, 0.24 mag brighter than the OB component. In contrast, a difference of 0.8 mag was assumed in Paper I.

The combined HST and radio datasets indicate that the OB companion possesses a powerful stellar wind, with a giant or supergiant luminosity class. Recent optical spectroscopy supports a supergiant O8 classification (Dougherty et al. 2000). As discussed by Dougherty et al., a large distance to this system would result if the absolute magnitude of the companion was typical of late O supergiants (Conti & Alschuler 1971). Instead, we adopt the distance of 1.4 kpc, as derived by Dougherty et al. At this distance, WR146 would

Table 4. Summary of the WC model atoms, and source of atomic datasets. N_F is the number of full levels, N_S the number of super levels and N_{TRANS} the corresponding number of transitions. The last column refers to the upper level of a given ion included in our treatment

| Species | N_F | N_S | N_{TRANS} | Ref | Details |
|----------------|-------|-------|--------------------|-----|--|
| He I | 39 | 27 | 315 | a | $n \leq 14$ |
| He II | 30 | 13 | 435 | b | $n \leq 30$ |
| He III | 1 | 1 | | | |
| C II | 88 | 39 | 791 | c,d | $nl \leq 2p3d$ $^4D^o$ |
| C III | 243 | 99 | 5513 | e,f | $nl \leq 2p4d$ $^1D^o$ |
| C IV | 64 | 49 | 1446 | g | $n \leq 30$ |
| C V | 1 | 1 | | | |
| O II | 3 | 3 | 3 | e,h | $nl \leq 2p3$ $^2P^o$ |
| O III | 50 | 50 | 213 | e,i | $nl \leq 2p4f$ 1D |
| O IV | 72 | 30 | 835 | e,j | $nl \leq 2p3p$ $^2P^o$ |
| O V | 91 | 31 | 748 | e,k | $nl \leq 2p4p$ 3P |
| O VI | 19 | 13 | 72 | g | $n \leq 5$ |
| O VII | 1 | 1 | | | |
| Si IV | 28 | 17 | 129 | h | $n \leq 6$ |
| Si V | 1 | 1 | | | |
| Fe IV | 280 | 21 | 5055 | l | $nl \leq 3d^4$ (1G) $4p^2P^o$ |
| Fe V | 182 | 19 | 2517 | m | $nl \leq 3d^3$ (2D) $4p^1P^o$ |
| Fe VI | 80 | 10 | 722 | n | $nl \leq 3d^2$ (1S) $4p^2P^o$ |
| Fe VII | 153 | 14 | 1213 | o | $nl \leq 3p^5$ (2P) $3d3$ ($b^2D^1P^o$) |
| Fe VIII | 1 | 1 | | | |
| 1299 440 20007 | | | | | |

(a) Fernley et al. (1987); (b) Wiese et al. (1966); (c) Yu Yan et al. (1987); (d) Yu Yan & Seaton (1987); (e) Nussbaumer & Storey (1983, 1984); (f) P.J. Storey (unpublished); (g) Peach et al. (1988); (h) Seaton (1995); (i) Luo et al. (1989); (j) Luo & Pradhan (1989); (k) Tully et al. (1990) (l) Becker & Butler (1995b); (m) Becker & Butler (1992); (n) Becker & Butler (1995a); (o) K. Butler (unpublished)

be a foreground object to Cyg OB2 (Lundstrom & Stenholm 1984; Torres-Dodgen et al. 1991).

We derived $E_{B-V}=2.87$ mag and $R=2.9$ using the optical-IR reddening law of Steenman & Thé (1989, 1991). This provided a superior comparison between theoretical predictions and de-reddened observations than with either the Howarth (1983) or Cardelli et al. (1989) laws. Therefore, $M_v = -5.3$ mag for the WCE component, by far in excess of ‘typical’ WCE stars (Smith et al. 1990).

4 MODELLING TECHNIQUE

Before discussing the fine analysis of each programme star, we introduce the spectroscopic technique followed here. We use the non-LTE code of Hillier & Miller (1998) which iteratively solves the transfer equation in the co-moving frame subject to statistical and radiative equilibria in an expanding, spherically symmetric and steady-state atmosphere. Relative to earlier versions of this code (Hillier 1987, 1990), two major enhancements have been incorporated, of particular relevance to WC-type stars, namely (i) line blanketing, (ii) clumping. Specific details of the techniques used are provided by Hillier & Miller (1998, 1999), with only a brief overview given here.

As discussed by Hillier & Miller (1998, 1999), extremely

complex atomic models are necessary for the quantitative analysis of WC stars, a computationally demanding requirement. Consequently, we make use of the technique of ‘super-levels’, in which several atomic levels of similar energies and properties are combined into a single one, a super level, with the populations of the super level calculated in the rate equations. Populations of individual atomic levels are then calculated by assuming that it has the same departure coefficient as the corresponding super level to which it belongs. In this way, extremely complex atoms of helium, carbon, oxygen and iron can be considered. In Table 4 a total of 1299 full (N_F) atomic levels are combined to produce just 440 super levels (N_S). The number of iron transitions is limited by $gf \leq 10^{-4}$, so that a total of 20,007 transitions are included. In addition to the specific models discussed here, we have also considered cases with expanded atomic datasets and ionization stages (e.g. Fe III), for which the differences in emergent synthetic spectrum were negligible.

Oscillator strengths, collision and photoionization cross-sections are taken from a wide variety of sources (Table 4). The OPACITY project (Seaton 1987, 1995) formed the basis of most radiative rates, supplemented by calculations for CNO by Nussbaumer & Storey (1983, 1984) and Storey (unpublished), and for iron by Becker & Butler (1992, 1995ab) and Butler (unpublished).

The stellar radius (R_*) is defined as the inner boundary of the model atmosphere and is located at Rosseland optical depth of 10 with the stellar temperature (T_*) defined by the usual Stefan-Boltzmann relation. Similarly, $T_{2/3}$ relates to the radius ($R_{2/3}$) at which the Rosseland optical depth equals 2/3.

Although the majority of spectral analyses of WR stars have adopted a standard $\beta=1$ velocity law, there is both observational and theoretical evidence for a more slowly accelerating outflow (e.g. Schmutz 1997; Lepine & Moffat 1999). Consequently, we adopt a form for the velocity law (Eqn 8 from Hillier & Miller 1999) such that two exponents are considered with the result that acceleration is modest at small radii, but continues to large distances, i.e.

$$v(r) = \frac{v_0 + (v_\infty - v_{\text{ext}} - v_0)(1 - R_*/r)^{\beta_1} + v_{\text{ext}}(1 - R_*/r)^{\beta_2}}{1 + (v_0/v_{\text{core}})(\exp((R_* - r)/h_{\text{eff}}))}$$

Here v_{ext} is an intermediate terminal velocity, v_{core} the core velocity (typically a few km s^{-1}), v_0 is the photospheric velocity (typically 100.0 km s^{-1}), v_∞ is the final wind velocity and h_{eff} the scale height ($\sim 0.01R_*$). For all models, we take $\beta_1=1$ and $\beta_2=50$ as in Hillier & Miller (1999).

There is now overwhelming evidence for the clumped nature of WR stars (e.g., Moffat et al. 1988; Moffat 1999), so we have adopted a simple filling factor approach. We assume that the wind is clumped with a volume filling factor, f , and that there is no inter clump material. Since radiation instabilities are not expected to be important in the inner wind we parameterise the filling factor so that it approaches unity at small velocities. Clumped and non-clumped spectra are very similar, except that line profiles are slightly narrower with weaker electron scattering wings in the former. Although non-clumped models can be easily rejected, because of the severe line blending in WC winds \dot{M}/\sqrt{f} is derived by our spectroscopic analysis, rather than \dot{M} and f . Also, this formulation introduces a revision of the BRA88 analytical formula, which will be addressed in Sect 5.

5 SPECTROSCOPIC ANALYSIS OF INDIVIDUAL STARS

In this section, we discuss the analysis of our programme WC stars. Stellar parameters (T_* , $\log L/L_\odot$, \dot{M}/\sqrt{f} , C/He, O/He) were adjusted until the observed ionization balance, line strengths and de-reddened optical continuum flux distribution were reproduced. Because of the substantial effect that differing mass-loss rates, temperatures and elemental abundances have on the emergent spectrum, this was an iterative process, in which initial model parameters were adopted from the literature if available (e.g. Koesterke & Hamann 1995; Morris et al. 1993). Terminal wind velocities are tabulated in Table 1.

The wind ionization balance was ideally selected on the basis of isolated optical lines from adjacent ionization stages of carbon and/or helium. In practice this was difficult to achieve because of the severe blending in WC winds. The low wind velocity of WR135 allowed He I $\lambda 5876$ and He II $\lambda 5412$ to be used as ionization balance constraints. In other cases, the wind ionization balance was selected on the basis of carbon diagnostics. Unfortunately, from all the possible WC diagnostics, the usual classification lines C III $\lambda 5696$ /C IV $\lambda 5804$ are difficult to match, being so sensitive to minor stellar parameter changes. Consequently alternative diagnostics were sought. For WR90, our primary diagnostics were C III $\lambda 8500$ /C IV $\lambda 7736$ since these suffered from negligible contamination and are predicted by the model to vary smoothly across the temperature space. In the case of WR146 this spectral region, as well as lines of low ionization, were not available. We selected He II $\lambda 5412$ /He I $\lambda 10830$, and C III $\lambda 6740$ /C IV $1.74\mu\text{m}$ as our primary ionization diagnostics.

Our experience with a variety of stellar models led us to select the strong ultraviolet P Cygni profiles of carbon (C III $\lambda 1909$, 2297) as our principal mass-loss diagnostics. A major limitation with C IV $\lambda 1550$ was that different mass-loss rates also affected nearby Fe lines, which strongly modulated the predicted strength of the emergent P Cygni profile. Since ultraviolet observations of WR146 are unavailable, we relied on He I $\lambda 10830$ as the principal mass-loss diagnostic in that case.

As in other recent spectroscopic studies of WC stars, He II $\lambda 5412$ /C IV $\lambda 5471$ were selected as the diagnostics for C/He determinations since the relative strength of these features are insensitive to differences of temperature or mass-loss rate. As discussed by Hillier & Miller (1998), this spectral region also contains a number of additional weak features, common to all stars. More problematic is that misleading C/He ratios would be obtained if (i) a limited number of C IV atomic levels were included; (ii) homogeneous models were adopted in which electron scattering wings were incorrectly predicted.

Test calculations were also performed using recombination theory. Comparisons of C/He with our more sophisticated results for WCE stars was found to be reasonable – we obtain C/He=0.08 by number for WR146 in this study, in accord with the value obtained by Eenens & Williams (1992) based on IR recombination lines. WCL stars are more problematic since recombination coefficients for C III are not available. In addition, the fraction of recombined helium is

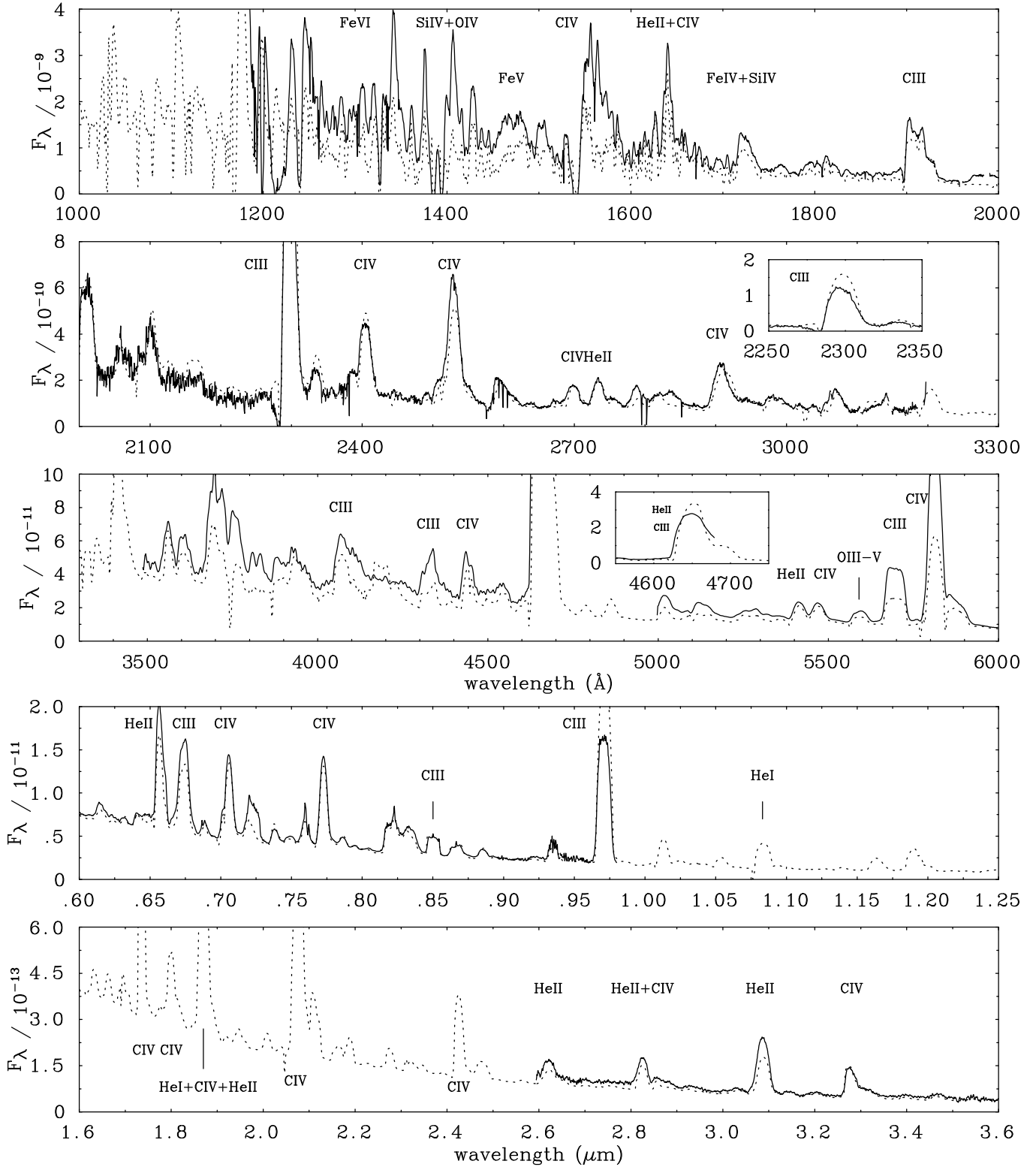


Figure 1. Comparison between de-reddened ($E_{B-V}=0.38$, $R=3.1$) spectrophotometry of HD 156385 = WR90 (WC7) obtained from IUE, CTIO, AAT and ISO (solid lines), and line-blanketed, clumped model predictions (dotted lines). Stellar parameters are $\dot{M}=2.5 \times 10^{-5} M_\odot \text{ yr}^{-1}$, $T_* = 71 \text{ kK}$, $\log L/L_\odot = 5.5$, $C/\text{He}=0.25$ and $O/\text{He}=0.03$ by number. Flux units are in ergs/cm²/s/Å

not straightforward to assess in such studies, so that helium abundances could be underestimated.

Oxygen abundances were more difficult to constrain, as already discussed by Hillier & Miller (1999), with the principal diagnostic region spanning $\lambda\lambda 2900\text{--}3500$. Since this spectral region was absent for WR146, we adopted C/O=4 by number, as predicted by current stellar evolutionary models. Note that our neon abundance determination in Sect. 7 is relatively insensitive to the precise oxygen content. Regarding silicon and iron, we adopt solar abundances since all distances are ≤ 2 kpc.

We now proceed to discuss individual stars in detail.

5.1 HD 156385 (WR 90)

The principal datasets for WR90 comprised HIRES IUE ultraviolet spectroscopy and AAT/RGO spectrograph optical observations. Secondary datasets were the blue CTIO spectroscopy from Torres-Dodgen & Massey (1988) and the 2.6-5 μm ISO spectroscopy (longer wavelength data were of insufficient S/N to be used as stellar diagnostics). The combined, UV-optical-IR flux calibrated dataset for WR90 allowed a well constrained reddening of $E_{B-V}=0.38$ mag, in agreement with the determination by Morris et al. (1993) (see Table 3). A distance of 1.55 kpc is implied from our assumed WC7 M_v -calibration.

The difficulty in identifying the stellar continuum in the rich emission line spectrum of WC stars makes rectification imprecise, as emphasised by Hillier & Miller (1998, 1999). Fig. 1 demonstrates the excellent agreement between the line and continuum distribution of the model spectrum (dotted lines) and observations (solid lines), and includes the true theoretical continuum distribution (dashed lines). The number of line features that are poorly reproduced is small, and includes C III $\lambda 5696$ (too weak), $\lambda 9710$ (too strong), plus C IV $\lambda 1548\text{--}51$, Si IV $\lambda 1393\text{--}1402$ (both too weak because of Fe-absorption) and O VI $\lambda\lambda 3811\text{--}34$ (too weak). The use of absolute fluxes appears to give poor results in the line strengths around C III $\lambda 2297$ since the de-reddened and theoretical continuum do not exactly match.

Our analysis reveals stellar parameters of $T_* = 71,000\text{K}$, $\log(L/L_\odot) = 5.5$ and $\dot{M}/\sqrt{f} = 8 \times 10^{-5} M_\odot \text{yr}^{-1}$. Adopting a volume filling factor of $f = 0.1$ indicates $\log \dot{M}/(M_\odot \text{yr}^{-1}) = -4.6$ and a wind performance number of ~ 8 . Use of C IV $\lambda 5471/\text{He II } \lambda 5412$ revealed C/He = 0.25 ± 0.05 by number. An oxygen abundance of O/He = 0.03 ± 0.01 by number was obtained by matching O IV $\lambda\lambda 2916\text{--}26$, $\lambda\lambda 3063\text{--}72$, and $\lambda 3560\text{--}63$.

5.2 HD 192103 (WR 135)

A substantial observational dataset was available for the WR135 analysis, particularly high quality UV (HIRES IUE), optical (INT), near-IR (INT, UKIRT) and mid-IR (ISO) spectrophotometry. An interstellar reddening of $E_{B-V} = 0.37$ was obtained for WR135, in accord with Smith et al. (1990) (see Table 3), but 0.18 mag lower than the more recent determination of Morris et al. (1993). Membership of Cyg OB3 implied an absolute visual magnitude of $M_v = -4.3$ mag.

Dereddened spectroscopy of WR135 (solid lines) is compared to our final synthetic model (dotted lines) in Figure 3.

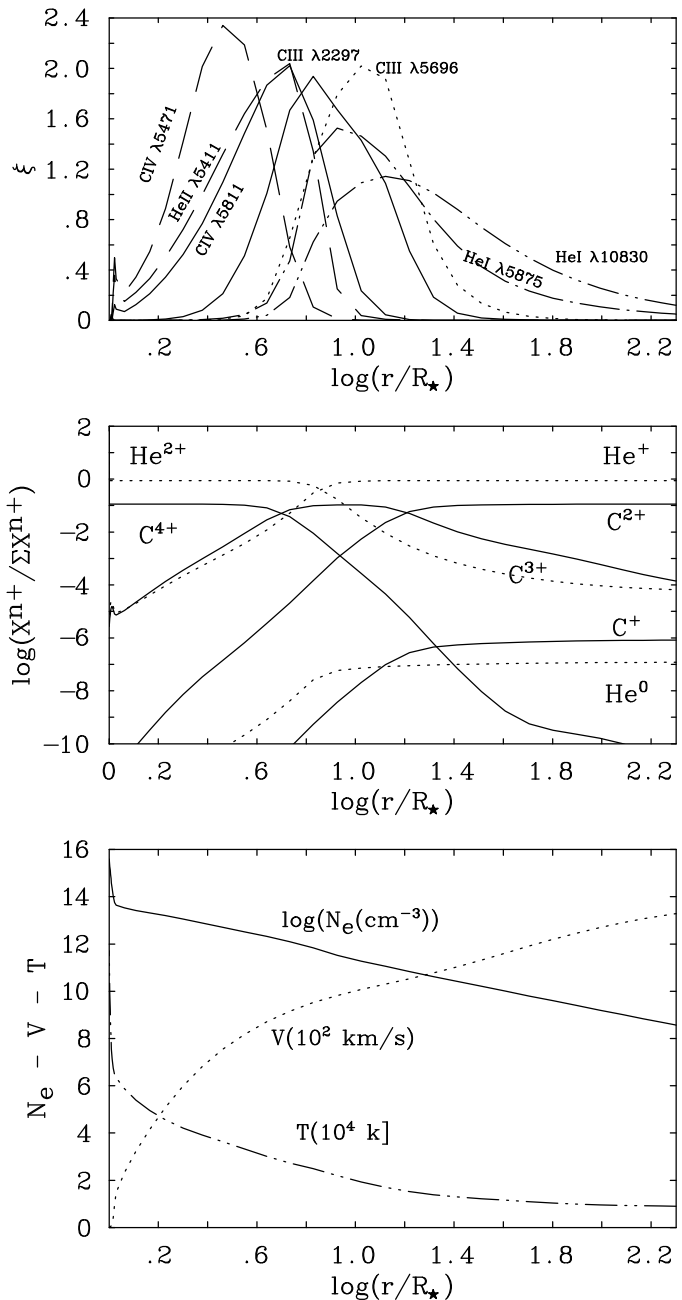


Figure 2. Model predictions for the WC8 star WR135, analysed in Section 5.2 (**Top**): Line formation regions for a selection of lines. The parameter ξ is related to the observed flux emitted in the corresponding line, and defined as in Hillier (1987). The integral of ξ over $d\log(r/R_*)$ is proportional to the equivalent width. (**Middle**): Wind ionization stratification for carbon (solid) and helium (dotted). Note that helium does not recombine to its neutral state in the outer wind. (**Bottom**): Radial dependence of electron temperature (kK, dot-dash), density (cm^{-3} , solid), and wind velocity (km s^{-1} , dotted)

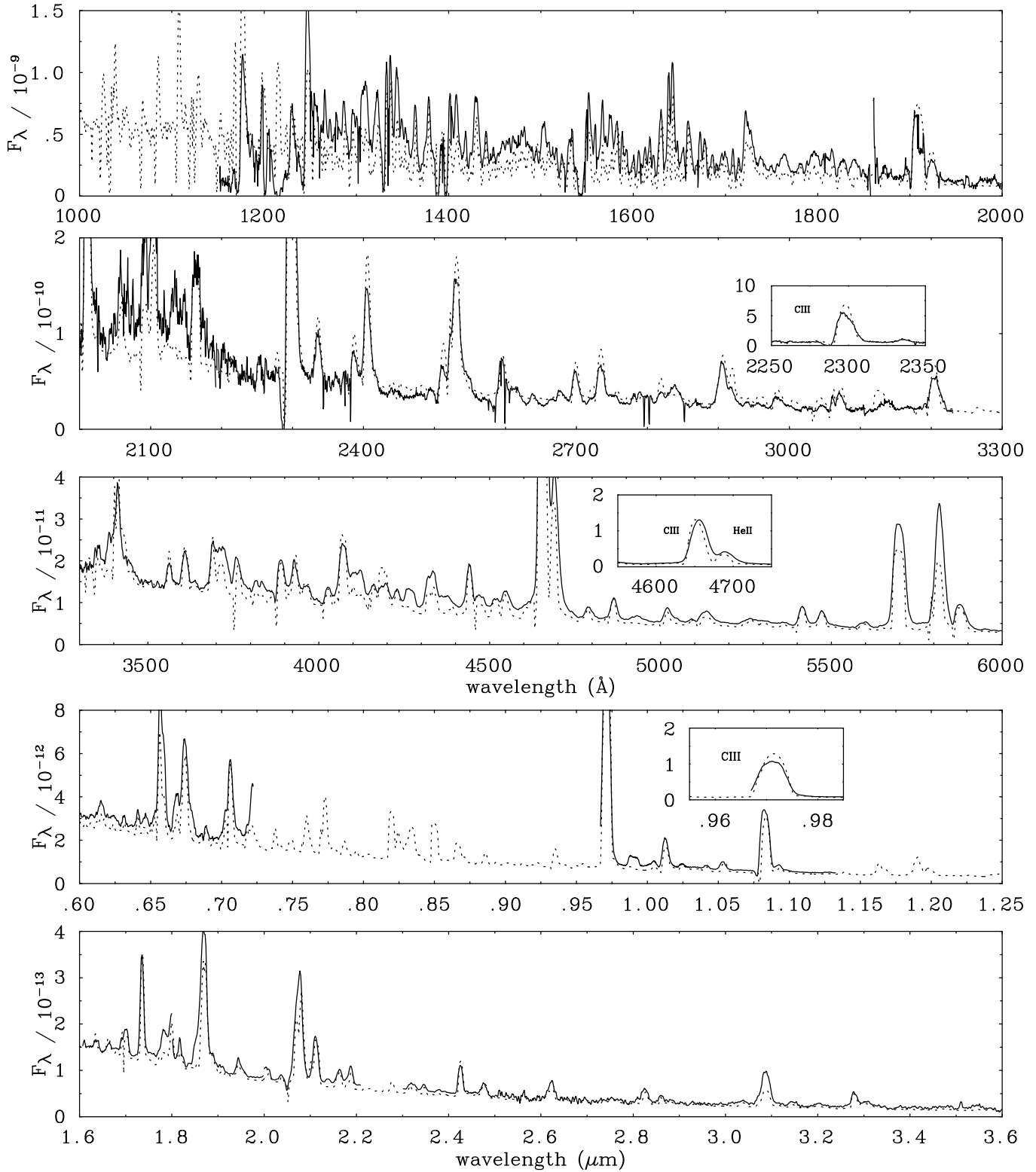


Figure 3. Comparison between the de-reddened ($E_{B-V}=0.37$ and $R=3.1$) spectrophotometry of HD 192103 = WR135 (WC8) obtained from IUE, INT, UKIRT and ISO (solid lines) and line-blanketed, clumped model predictions (dotted lines). Stellar parameters are $\dot{M}=1.3 \times 10^{-5} M_\odot \text{ yr}^{-1}$, $T_* = 63 \text{ kK}$, $\log L/L_\odot = 5.20$, $C/\text{He}=0.13$ and $O/\text{He}=0.03$ by number. Flux units are in $\text{ergs}/\text{cm}^2/\text{s}/\text{\AA}$.

Agreement is overall excellent, even for the forest of iron lines in the UV. The relatively low wind velocity of WR135 permits a greater number of individual diagnostics to be selected, including He II $\lambda 4686$, He I $\lambda 5876$, so that the derived properties can be treated with confidence. Indeed, C III $\lambda 5696$ and C IV $\lambda 5804$ are fairly well matched in this case. The strong C III spectral features at $\lambda 2297$ and $\lambda 9710$ are predicted to be 20–30% too strong. Other notable model deficiencies include underestimating the strength of C II emission at $\lambda 4267$, $\lambda 9900$, and O VI $\lambda \lambda 3811$ –34, with O III $\lambda 3130$ too strong. As with WR90, the use of absolute fluxes, appears to give poor results in the line strengths around He II $\lambda 2530$ since the de-reddened and theoretical continuum do not exactly match. This discrepancy simply reflects the inadequacy of the adopted reddening law, rather than a fundamental flaw with current models.

We obtain the following stellar parameters: $T_* = 63$ kK, $\log(L/L_\odot) = 5.2$ and $\dot{M}/\sqrt{f} = 3.8 \times 10^{-5} M_\odot \text{ yr}^{-1}$. Adopting a volume filling factor of $f = 0.1$ indicates $\log \dot{M}/(M_\odot \text{ yr}^{-1}) = -4.9$ and a wind performance number of ~ 8 . Use of C IV $\lambda 5471$ /He II $\lambda 5412$ revealed C/He = 0.13 ± 0.03 by number. Once again, the oxygen abundance is poorly constrained, although O/He = 0.03 ± 0.01 provides a reasonable match to O IV $\lambda \lambda 2916$ –26 and $\lambda \lambda 3063$ –72, with O III $\lambda 3127$ too strong.

In Fig. 2, we present the wind structure of the final WR135 synthetic model, including line formation regions, ionization balance etc. Similar relations are shown for WR111 (WC5) in Hillier & Miller (1999).

5.3 WR 146

Our principal observational datasets for WR146 are identical to those used in Paper I, namely INT (optical), UKIRT (near-IR) and ISO (2.6–5 μm because of the low S/N at longer wavelengths). The difference in our approach is to derive stellar and chemical properties solely from spectral synthesis, rather than recombination theory and independent modelling of the continuum. As discussed in Sect. 3.2, we follow the distance estimate of 1.4 kpc from Dougherty et al. (2000), in the light of new observations from Niemela et al. (1998).

We have included the spectral energy distribution of a O8 supergiant in our synthesis, using that for HD 151804 (O8 If) derived by Crowther & Bohannan (1997). The IR free-free excess of this model is somewhat greater than equivalent temperature Kurucz (1991) models for which the lowest gravity available is $\log g = 4$. Because of the contamination from the late O supergiant, the line spectrum of the WC component of WR146 is relatively weak, as shown in Fig. 4. The flux level of the O companion, the contribution of which declines with increasing wavelength, is illustrated as a dashed line in Fig. 4. Comparison between de-reddened observations and our synthetic spectrum is excellent, with the notable exception of C IV $\lambda 5804$.

Our final stellar parameters for the WC5 star were, $T_* = 57$ kK, $\log L/L_\odot = 5.7$, and $\dot{M}/\sqrt{f} = 1 \times 10^{-4} M_\odot \text{ yr}^{-1}$. A filling factor of $f = 0.1$ reproduced the red wing of C III–IV $\lambda 4650$ –He II $\lambda 4686$. The high wind velocity of WR146 meant that C IV $\lambda 5471$ /He II $\lambda 5412$ were blended. Nevertheless, we were able to constrain the carbon content, deriving C/He = 0.08 ± 0.02 by number, a factor of two times lower than that estimated in Paper I from recombination

line analysis, but now in accord with Eenens & Williams (1992). Oxygen is extremely difficult to measure in WR146 since the usual near-UV diagnostics are unavailable, so that O/He = 0.02 ± 0.01 is adopted.

Finally, should the absolute magnitude of WR146 be more typical of other WCE stars, namely $M_v = -3.7$ mag (Smith et al. 1990), what would be the effect on the derived stellar parameters? In this case, our reddening towards WR146 would imply a distance of 660 pc, such that the companion star would be extremely faint $M_v = -3.5$ mag, typical of an early B dwarf. The stellar properties of WR146 would be unchanged, except that $\log L/L_\odot = 5.0$, and $\dot{M}/\sqrt{f} = 3.3 \times 10^{-5} M_\odot \text{ yr}^{-1}$. In this case it would be difficult to reconcile these properties with the HST/radio observations of WR146 (Dougherty et al. 1996; Niemela et al. 1998).

6 SUMMARY OF SPECTROSCOPIC RESULTS

In this section we discuss the results of our quantitative analyses, and make comparisons with previous studies.

6.1 Stellar parameters of WC stars

In Table 5, we provide a summary of the derived properties of our programme WC stars, including results for WR11 and WR111 from De Marco et al. (2000) and Hillier & Miller (1999), obtained using identical techniques. Despite our sample spanning WC5 to WC8, there is no obvious trend between spectral type and stellar temperature. Indeed, the WC5 component of WR146 is found to have the lowest stellar temperature, although this is certainly a most unusual WCE star! The subtle behaviour of C III 5696\AA and C IV 5808\AA from our modelling indicates that, unfortunately, we are unable to use these as probes of wind ionization for WC5–8 stars (while we cannot obtain a simultaneous fit to both lines, a relatively small change in parameters can lead to a fit of either line).

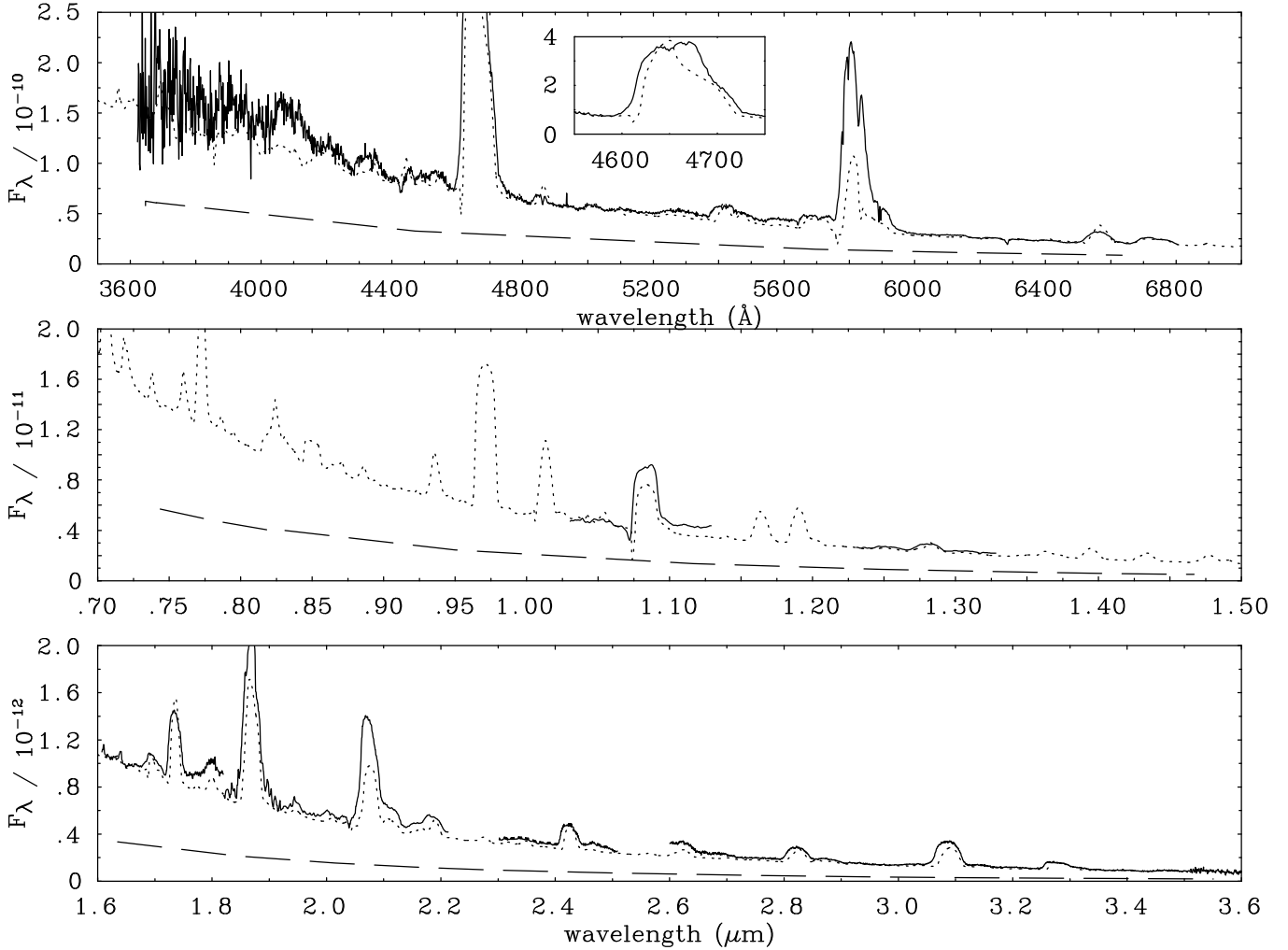
Similarly, although there is considerable spread in carbon abundances, WR146 exhibits the lowest carbon mass fraction, in contrast to the predicted increase in C/He ratio at earlier spectral type. Koesterke & Hamann (1995) derived a broad range of C/He ratios at each spectral type for WC5–8 stars.

How do the present line blanketed, clumped results compare with previous studies? Unfortunately, WR135 is the sole programme star that has been the subject of quantitative studies in the past. Eenens & Williams (1992) derived elemental abundances from IR recombination lines, estimating C/He = 0.12 by number, in excellent agreement with our determination of 0.13. Howarth & Schmutz (1992) used a pure helium non-LTE model analysis to investigate WR135 based solely on 1 μm spectroscopy. Since pure helium models are expected to be inadequate for WC analyses, Koesterke & Hamann (1995) considered both carbon and helium in their study of WC stars, including WR135.

In Table 6 we compare results from our present analysis of WR135 with these previous studies, scaling their results to our absolute visual magnitude. Wind velocities and \dot{M}/\sqrt{f} are in relatively good agreement, while the effect of including carbon and blanketing has a dramatic effect on

Table 5. Derived stellar properties for programme WC stars, including results obtained by De Marco et al. (2000) for WR11 and Hillier & Miller (1999) for WR111 for comparison

| WR | Spectral Type | T_* kK | $T_{2/3}$ kK | $\log(L/L_\odot)$ | v_∞ km s $^{-1}$ | $\log \dot{M}$ M $_\odot$ yr $^{-1}$ | \dot{M}/\sqrt{f} $10^{-5}M_\odot$ yr $^{-1}$ | C/He # | O/He # | $\log Q_{H^0}$ s $^{-1}$ | $\log Q_{He^0}$ s $^{-1}$ | M_v (WC) mag |
|-----|---------------|-------------|-----------------|-------------------|----------------------------|---|---|-----------|-----------|-----------------------------|------------------------------|-------------------|
| 11 | WC8+O7.5III | 57 | 51 | 5.0 | 1550 | -5.1 | 2.9 | 0.15 | 0.03 | 48.8 | 47.8 | -3.7 |
| 90 | WC7 | 71 | 29 | 5.5 | 2045 | -4.6 | 8.0 | 0.25 | 0.03 | 49.3 | 48.7 | -4.7 |
| 111 | WC5 | 91 | 30 | 5.3 | 2300 | -4.8 | 4.7 | 0.4 | 0.10 | 49.2 | 48.5 | -4.2 |
| 135 | WC8 | 63 | 27 | 5.2 | 1400 | -4.9 | 3.8 | 0.13 | 0.03 | 49.1 | 48.3 | -4.3 |
| 146 | WC5+O8 | 57 | 33 | 5.7 | 2700 | -4.5 | 10.5 | 0.08 | 0.02 | 49.6 | 48.7 | -5.3 |

**Figure 4.** Comparison between the de-reddened ($E_{B-V}=2.87$ mag, $R=2.9$) spectrophotometry of WR 146 (WC5+OB) obtained from INT, UKIRT and ISO (solid lines) and line-blanketed, clumped model predictions (dotted lines). The contribution of the late O companion is taken into consideration, using model calculations by Crowther & Bohannan (1997) – its continuum distribution is indicated with dashed-lines. WC stellar parameters are $\dot{M}=3.3 \times 10^{-5} M_\odot \text{ yr}^{-1}$, $T_*=57$ kK, $\log L/L_\odot = 5.7$, C/He=0.08 and O/He=0.02 by number. Flux units are in ergs/cm 2 /s/Å.

the stellar temperatures and luminosities, such that the luminosity derived here is a factor of two times higher than Howarth & Schmutz (1992), who adopted a stellar temperature of 35,000K.

Stellar parameters are in much better agreement with

Koesterke & Hamann (1995). They compared specific line strengths with model grids at fixed C/He ratio, and chose simple model atoms of He I-II and C II-IV. Although spectral comparisons between model predictions and observations were not presented by Koesterke & Hamann (1995),

the fit quality was judged to be poor, with large discrepancies for the C III $\lambda 5696$ and $\lambda 6740$ lines. Therefore, we have greater confidence in our results since detailed UV, optical and IR synthetic spectrophotometry compare favourably with observations.

From Table 6, blanketing and clumping conspire to revise the wind performance number, $\dot{M}/v_\infty/(L/c)$, from 30 in the study of Koesterke & Hamann (1995) to just 5 for WR135! For our entire sample, performance numbers are ≤ 10 , with previous studies indicating values of up to 100 (Howarth & Schmutz 1992; Koesterke & Hamann 1995).

6.2 Evolutionary status

The wide range in stellar luminosity of our sample of WC stars, $L/L_\odot = 10^5$ to $10^{5.7}$, implies a considerable range in current stellar masses. Following the mass-luminosity relation for hydrogen-free WR stars of Schaerer & Maeder (1992), present masses of $9M_\odot$ (WR135), $13M_\odot$ (WR90) and $19M_\odot$ (WR146) are implied. In contrast, initial mass estimates are much more dependent on specific evolutionary tracks.

All models predict stars to pass through the WC phase at ages of between 2.7–4.5 Myr. For initial 40 and $60M_\odot$ models, stellar masses during the early WC phase are predicted to be $\sim 14M_\odot$ and $\sim 24M_\odot$, respectively. At higher initial mass, the situation is extremely model dependent. For example, an evolutionary model with initial mass $120M_\odot$ will produce a $60M_\odot$ WC star using standard de Jager et al. (1988) mass-loss rates. Alternatively, a $10M_\odot$ WC star will result based on (2 \times) enhanced mass-loss for the post main-sequence and WNL phases (Schaller et al. 1992), or only a $4M_\odot$ WC star for (2 \times) enhanced mass-loss during the entire stellar evolution (Meynet et al. 1994). Therefore, the present masses and ages of our programme WC stars are well constrained, but initial masses are not.

In order to attempt estimates of initial masses, we compare our derived (C+O)/He ratios versus stellar luminosities with evolutionary predictions in Fig. 5. Predictions for 40– $120M_\odot$ initial models assume (2 \times) enhanced mass-loss relative to de Jager et al. (1988) during the entire stellar evolution (Meynet et al. 1994). These models favour $60M_\odot$ for WR146 and WR90 and $40M_\odot$ or $85M_\odot$ for WR135. Consequently, multiple initial mass estimates may result for individual stars. Nevertheless, we currently favour $40M_\odot$ for WR135 and $60M_\odot$ for WR146 and WR90.

Specific comparisons between the stellar properties of WR90, WR135 and WR146 and Meynet et al. (1994) evolutionary predictions are made in Table 7. Both the initial $60M_\odot$ and $85M_\odot$ models adopt mass-loss rates that exceed observations by large factors during early WC stages. This is because evolutionary models for hydrogen-free WR stars adopt mass-loss rates that are solely functions of mass (Langer 1989). Clearly, future evolutionary models should take allowance for more appropriate WR mass-loss rates.

6.3 Radio fluxes

We now compare predicted radio fluxes from our spectroscopic mass-loss rates. Hillier & Miller (1999) provide a formulation based on Eqn 9 in Wright & Barlow (1975), allowing for the filling factor according to Abbott et al. (1981).

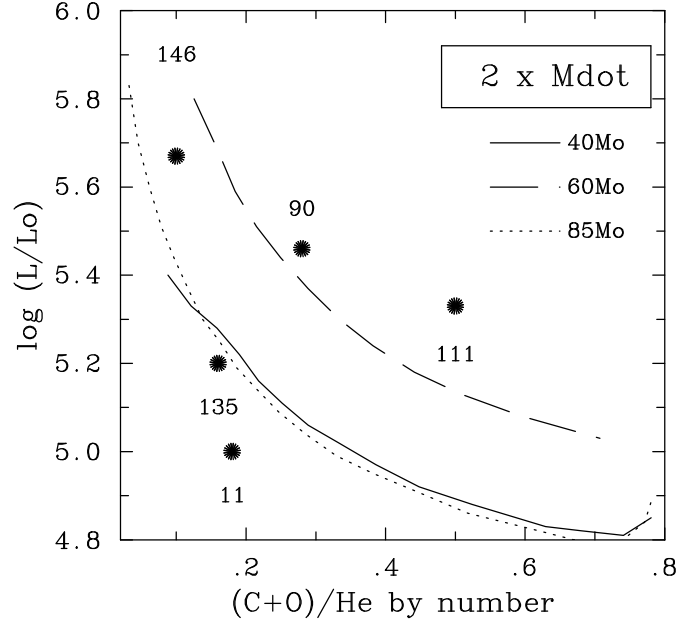


Figure 5. Comparison of measured (C+O)/He ratios versus luminosities for our programme stars, including WR111 (WC5) from Hillier & Miller (1999), with theoretical expectations from the solar metallicity evolutionary tracks assuming enhanced (2 \times) mass-loss (Meynet et al. 1994)

Table 6. Comparison of our derived stellar parameters for WR135 with Howarth & Schmutz (1992, HS92) and Koesterke & Hamann (1995, KH95). We have adjusted their parameters to our assumed visual absolute magnitude ($M_v = -4.3$ mag)

| Ref. | Model | $\log(L/L_\odot)$ | T_* kK | v_∞ km s $^{-1}$ | \dot{M}/\sqrt{f} M_\odot yr $^{-1}$ | C/He |
|-----------|-----------|-------------------|-------------|----------------------------|--|------|
| HS92 | He | 4.9 | (35) | 1500 | 5×10^{-5} | – |
| KH95 | He+C | 5.1 | 76 | 1300 | 6×10^{-5} | 0.14 |
| This work | He+C+O+Fe | 5.2 | 63 | 1400 | 4×10^{-5} | 0.13 |

In all cases, the dominant ionization at the outer boundary of our models, $N_e \sim 10^8$ cm $^{-3}$ or $200R_*$ is He $^+$, C $^{2+}$ and O $^{2+}$ (see Fig. 2). Since the radio emitting region lies at lower densities, we also consider cases in which C $^+$ and/or O $^+$ are dominant. Outer wind electron temperatures are typically 8000K (Fig. 2), except for WR146 for which the lower cooling produced by less metals implies 9000K.

We compare predicted radio fluxes with observed values taken from the literature in Table 8, in which a uniform UV/optical filling factor of $f=0.1$ has been adopted throughout. Note that the quoted radio flux for WR146 refers solely to the WC component (the southern mean emitted flux S_5 in Dougherty et al. 2000). We find that consistency is excellent for WR135 and WR146 for doubly ionized carbon and oxygen, while singly ionized carbon and oxygen are favoured for WR90. However, C $^+$ is not predicted to be the dominant ionization stage in the outer wind of these stars (Fig. 2), so that the predicted radio flux for this star appears to be too high.

It is possible that the filling factor in the radio and

Table 7. Comparison between our derived stellar parameters for WC stars and evolutionary predictions from Meynet et al. (1994)

| WR | M M_{\odot} | τ Myr | T_* kK | $\log(L/L_{\odot})$ | \dot{M} $M_{\odot} \text{ yr}^{-1}$ | C/He | O/He |
|------------------------------------|--------------------|---------------|-------------|---------------------|--|------|-------|
| 90 | | | 71 | 5.5 | 2.5×10^{-5} | 0.25 | 0.03 |
| 135 | | | 63 | 5.2 | 1.2×10^{-5} | 0.13 | 0.03 |
| 146 | | | 57 | 5.7 | 3.3×10^{-5} | 0.08 | 0.02 |
| — $M_{\text{init}}=40 M_{\odot}$ — | | | | | | | |
| 13 | 4.56 | 126 | | 5.4 | 5.5×10^{-5} | 0.08 | 0.004 |
| 8 | 4.72 | 122 | | 5.1 | 1.8×10^{-5} | 0.25 | 0.04 |
| — $M_{\text{init}}=60 M_{\odot}$ — | | | | | | | |
| 23 | 3.57 | 136 | | 5.8 | 24.6×10^{-5} | 0.12 | 0.01 |
| 12 | 3.67 | 131 | | 5.4 | 4.8×10^{-5} | 0.25 | 0.04 |
| — $M_{\text{init}}=85 M_{\odot}$ — | | | | | | | |
| 15 | 3.10 | 128 | | 5.5 | 9.1×10^{-5} | 0.07 | 0.004 |
| 8 | 3.30 | 120 | | 5.0 | 1.7×10^{-5} | 0.25 | 0.04 |

Table 8. Comparison between predicted and observed 6cm (4.9GHz) radio fluxes in our programme stars, assuming $f=0.1$ for the UV/optical line forming region. The filling factor entry in the table corresponds to the adopted value in the radio region, indicating the change in that quantity required to recover the observed flux at 4.9GHz. We have included WR11 in this table, since a neon abundance determination for this star is to be carried out in Sect. 7.2.

| WR | Ionization state | T_e kK | f radio | S_{ν}^{cm} (mJy) Pred. | Obs.(Ref) |
|-----|---|-------------|--------------|--------------------------------------|-----------|
| 11 | He ⁺ C ²⁺ O ²⁺ | 8 | 0.10 | 20.5 | |
| | He ⁺ C ²⁺ O ²⁺ | 8 | 0.05 | 32.5 | 32.2 (a) |
| | He ⁺ C ²⁺ O ⁺ | 8 | 0.10 | 20.2 | |
| | He ⁺ C ⁺ O ⁺ | 8 | 0.10 | 15.1 | |
| 90 | He ⁺ C ²⁺ O ²⁺ | 8 | 0.10 | 1.72 | |
| | He ⁺ C ²⁺ O ²⁺ | 8 | 0.20 | 1.08 | 1.10 (b) |
| | He ⁺ C ²⁺ O ⁺ | 8 | 0.10 | 1.64 | |
| | He ⁺ C ⁺ O ⁺ | 8 | 0.10 | 1.10 | |
| 135 | He ⁺ C ²⁺ O ²⁺ | 8 | 0.10 | 0.54 | 0.60 (a) |
| | He ⁺ C ²⁺ O ⁺ | 8 | 0.10 | 0.51 | |
| | He ⁺ C ⁺ O ⁺ | 8 | 0.10 | 0.40 | |
| 146 | He ⁺ C ²⁺ O ²⁺ | 9 | 0.10 | 2.04 | 2.00 (c) |
| | He ⁺ C ²⁺ O ²⁺ | 9 | 0.20 | 1.29 | |
| | He ⁺ C ²⁺ O ²⁺ | 9 | 0.30 | 0.98 | |
| | He ⁺ C ²⁺ O ⁺ | 9 | 0.10 | 1.95 | |
| | He ⁺ C ⁺ O ⁺ | 9 | 0.10 | 1.65 | |

a: Leitherer et al (1997), b: Abbott et al. (1986), c: Dougherty et al. (2000)

optical forming regions differs significantly. The predicted radio flux of WR90 would be in excellent agreement with the observed value if the radio filling factor was ~ 0.2 , while that of WR11 requires ~ 0.05 . Hillier & Miller (1999) found a similar discrepancy in their study of WR111. Note also that there is observational evidence that WR90 may not be single, since it is a non-thermal emitter (Leitherer et al 1997; Chapman et al 1999).

We also include calculations for WR11 in Table 8, since we attempt to re-derive its neon abundance determination

in Section 7. As for the other stars in our sample, possible variations in filling factor between the inner and outer wind are important.

7 NEON AND SULPHUR ABUNDANCES IN WC STARS

We are now in a position to determine neon abundances in our programme WC stars based on ISO spectroscopy, supplemented by sulphur determinations for WR11. In this section we first provide a revised formulation for the determination of neon in a clumped medium, following BRA88, and subsequently provide measurements for each star.

7.1 Ionic abundances from fine-structure lines in an inhomogeneous wind

We have re-derived the numerical and analytical forms for the determination of ionic abundances in clumped winds from BRA88. We consider a fine-structure line from ion i , with transition energy $h\nu_{ul}$. If D is the distance to the star and I_{ul} is the observed line flux, then

$$4\pi D^2 I_{ul} = \int_0^{\infty} n_u A_{ul} h\nu_{ul} 4\pi r^2 f dr \quad \text{erg s}^{-1} \quad (1)$$

where A_{ul} is the line transition probability and we have introduced the filling factor f into their formulation. n_u represents the density of ions in the upper level, and can be written as,

$$n_u = f_u n_i \quad \text{cm}^{-3} \quad (2)$$

where n_i is the species ion density and f_u is the fractional population of the upper level. Upper level populations, f_u , were determined for each ion by solving the equations of statistical equilibrium using EQUIB (Adams & Howarth, priv. comm) for ≥ 30 electron densities in the range 10^0 to 10^{12} cm^{-3} , and 9 electron temperatures covering 5k to 14kK. Thus,

$$n_u = \frac{f_u \gamma_i A}{f r^2} \quad \text{cm}^{-3} \quad (3)$$

where γ_i is the fraction of all ions represented by ion species i

$$\gamma_i = \frac{n_i}{\sum_j n_j} \quad (4)$$

and A is the mass loss parameter (Eqn 8 from BRA88). Combining equations 1–3, the filling factor term cancels out, leaving

$$I_{ul} = \frac{\gamma_i}{D^2} A_{ul} h\nu_{ul} A \int_0^{\infty} f_u(r, f, T) dr \quad \text{erg cm}^{-2} \text{s}^{-1} \quad (5)$$

We deviate from BRA88 by carrying out the integral in density, rather than radial space. Since $r(N_e)$ is a bijection, we can modify this integral so that the dependency of f_u on A and f (and hence \dot{M}) is removed from the integral term. Equation 5 can then be modified to:

$$\int_0^{\infty} f_u(r, f, T) dr = \sqrt{\frac{\gamma_e A}{4f}} \int_0^{\infty} \frac{f_u(N_e, T)}{N_e^{1.5}} dN_e \quad (6)$$

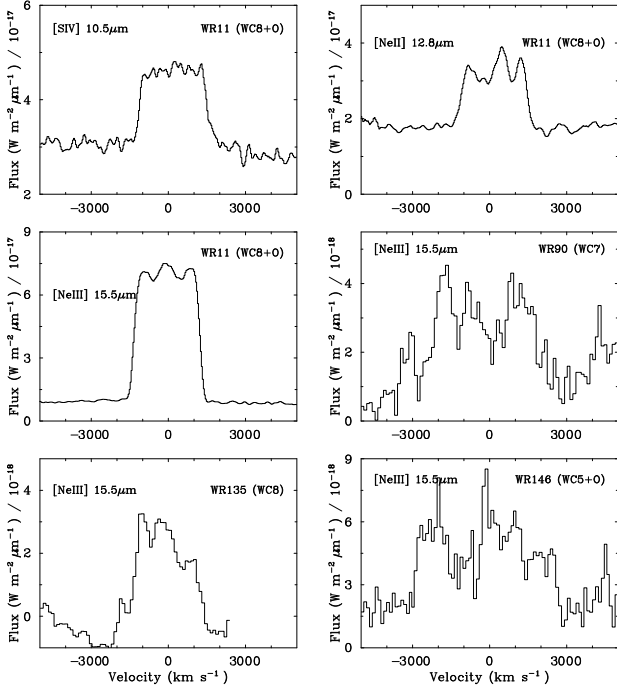


Figure 6. ISO/SWS observations of fine structure [SIV] $10.5\mu\text{m}$, [NeII] $12.8\mu\text{m}$ and [NeIII] $15.5\mu\text{m}$ emission in WR11, WR90, WR135 and WR146.

For a more straightforward numerical computation, Equation 6 is slightly adjusted:

$$\int_0^\infty \frac{f_u(N_e, T)}{N_e^{1.5}} dN_e = \ln(10) \int_0^\infty \frac{f_u(N_e, T)}{\sqrt{N_e}} d\log(N_e) \quad (7)$$

The effect of this modification leads to a significant improvement over BRA88, who used an average value for each region Δr , since the line formation region is a very sensitive function of f_u . Also, the dependence of the integral on \dot{M} is removed. Consequently, BRA88 overestimated the integral term, producing a lower elemental abundance. Our final numerical expression for the ion number fraction γ_i , is (cgs units):

$$\gamma_i = \frac{(4\pi\mu m_H v_\infty)^{1.5}}{\ln(10) f^{0.25}} \left(\frac{\sqrt{f}}{\dot{M}} \right)^{1.5} \frac{1}{F_u(T)} \frac{2D^2 I_{ul}}{\sqrt{\gamma_e} A_{ul} h\nu_{ul}} \quad (8)$$

with

$$F_u(T) = \int_0^\infty \frac{f_u(N_e, T)}{\sqrt{N_e}} d\log(N_e). \quad (9)$$

Provided radio and recombination processes are used to derive \dot{M}/\sqrt{f} , elemental abundances are only weakly dependent on the distance ($\propto D^{-0.25}$) since mass-loss rates depend on $D^{1.5}$. Therefore elemental abundances obtained with filling factors of $f=0.1$ or 1.0 differ by a factor of 1.8.

In order to allow for the possibility of a clumped medium, the analytical expression for the ion number fraction given by BRA88 (their equation A13) also needs to be multiplied by a factor of \sqrt{f} . We include determinations of γ_i using both the integral and analytical expressions in our

subsequent calculations. We find that the analytic expression is reliable to within $\sim 20\%$.

7.2 Neon abundances for WC stars

We are now in a position to evaluate neon abundances in our programme WC stars, using Equation 8. Figure 6 shows ISO/SWS observations of [NeIII] $15.5\mu\text{m}$ emission for each of our programme stars, together with [NeII] $12.8\mu\text{m}$ in WR11. Emission line fluxes are listed in Table 9.

Table 9 also includes atomic quantities used to derive ion fractions. Transition probabilities are taken from the NIST Atomic Spectra Database, while collision strengths are obtained from papers in the IRON Project series (see Table 9 for references). ISO flux measurements for WR11 compare closely with previous measurements from IRAS and ground-based observations (van der Hucht & Olmon (1985); BRA88), as indicated in Table 9.

In the following comparison, we include abundances derived from ISO mid-IR neon lines for WR11, using stellar parameters derived by De Marco et al. (2000).

Neon abundance determinations are sensitive to the ionization balance in the line forming region for the fine-structure lines, and is comparable to that of the radio forming continuum, $N_e \sim 10^5 \text{ cm}^{-3}$. Ne^+ , with an ionization potential that is higher than C^+ and O^+ , is observed solely in WR11 (WC8). Therefore, we have allowed for the possibility that the carbon and oxygen ionization balance are singly ionized for WC8 stars, with He^+ and doubly ionized carbon and oxygen otherwise. Table 10 shows predicted ion abundances of Ne^{2+} for each case, plus measured Ne^+ for WR11, with upper limits otherwise. In all cases $\text{Ne}/\text{He} \sim 3\text{--}4 \times 10^{-3}$ by number, significantly greater than the expected cosmic value of $\text{Ne}/\text{He} \sim 5 \times 10^{-4}$ in the C and O-enriched WC environment.

It is possible that neon exists in (unseen) higher ionization stages, specifically Ne^{3+} . However, the ionization potential for Ne^{3+} , 97eV, is significantly higher than C^{3+} (64eV) and O^{3+} (77eV) which are not expected to be present in the outer winds of WC stars (Fig. 2).

In summary, measurement of fine-structure lines of neon from ISO/SWS observations reveal $\text{Ne}/\text{He} = 0.003\text{--}0.004$ ($\text{Ne}/\text{C} \sim 0.02$), a factor of 6–8 times higher than cosmic abundances of $\text{Ne}/\text{He} = 0.0005$ for the carbon rich winds of WC stars, supported also by sulphur abundance determinations. However, what additional sources of uncertainty are there in our Ne/He determinations, and why do our results for WR11 differ from BRA88, who obtained $\text{Ne}/\text{He} = 0.001$?

Although the ISO-SWS neon line fluxes are in good agreement with the ground-based and IRAS neon line fluxes from BRA88 (Morris et al. 1998), we derive an elemental abundance that is *three* times higher. The source of this discrepancy is due to a different distance to WR11, and the use of a non-clumped mass-loss rate by BRA88. Morris et al. (2000) have recently emphasised the need for a reliable mass-loss rate estimate in the determination of neon abundances. In addition, our derived neon abundance is in good agreement with Morris et al. (1998) who combined ISO/SWS neon fluxes with the HIPPARCOS distance to WR11, and the X-ray derived mass-loss rate of Stevens et al. (1996).

The other major factor affecting neon abundances is clumping. Our UV/optical analyses use filling factors of

$f=0.1$, yet we cannot observationally constrain the filling factor to better than $0.05 \leq f \leq 0.25$, indicating a further 20% uncertainty in Ne/He. Of greater importance, we assume identical filling factors for the optical line forming region ($\approx 10^{11} \text{ cm}^{-3}$) and the neon emitting region ($\approx 10^5 \text{ cm}^{-3}$). Neon abundances would be increased by 40% for WR90, decreased by 30% for WR11, with WR146 and WR135 unchanged, assuming that (i) UV/optical mass-loss rates are fully consistent with radio fluxes (recall Sect. 6.3), and that (ii) volume filling factors in the neon emitting region are identical to those in the radio region.

7.3 Sulphur abundances for WR11

In order to assess the reliability of our derived abundances, we have also calculated the sulphur abundance for WR11 based on ISO observations of fine-structure [S IV] $10.5\mu\text{m}$ and [S III] $18.7\mu\text{m}$ lines (Table 9). Since sulphur is not enhanced by nucleosynthesis, abundances should correspond to the cosmic value. The line forming region for the sulphur fine-structure lines peaks at $N_e \sim 10^4 \text{ cm}^{-3}$, somewhat lower than the neon lines.

ISO spectroscopy of [S IV] $10.5\mu\text{m}$ confirms the line flux measured from ground-based spectroscopy by BRA88, while stellar modelling anticipates weak contamination from lines of He I (12–8) $10.52\mu\text{m}$ and C III (20–17) $10.54\mu\text{m}$. The stellar analysis of WR11 by De Marco et al. (2000) predicts a 15% contribution from these lines to the observed flux, which has been corrected accordingly. For the first time in a Wolf-Rayet star, ISO reveals the presence of [S III] $18.7\mu\text{m}$, blended with the stellar He I (14–10) $18.62\mu\text{m}$ feature, resulting in a 30% decrease in [S III] flux. Use of an inappropriate mass-loss rate and distance for WR11 led BRA88 to suggest $S^{3+}/\text{He} = 2.5 \times 10^{-5}$, such that they were obliged to predict $S^{2+} > S^{3+}$, with an expected high [S III] $18.7\mu\text{m}$ line flux that is not confirmed by ISO observations.

From Table 10, we find $\gamma_{S^{2+}} = 1.9 \times 10^{-5}$ and $\gamma_{S^{3+}} = 3.1 \times 10^{-5}$, which imply $S/\text{He} = 6 \times 10^{-5}$ by number. This is in good agreement with the cosmic value of 7.5×10^{-5} for the C and He enriched environment of WR11. Therefore, our determinations imply $\text{Ne}/S = 50$ for WR11, a factor of eight times greater than the cosmic value of $\text{Ne}/S \sim 7$. Since these lines are formed in similar regions of the stellar wind, Ne/S abundances are essentially independent of clumping, and reveal a degree of neon enrichment relative to sulphur that is equivalent to that derived earlier for He.

7.4 Comparison of abundances with theoretical predictions

Regarding theoretical expectations, the level of neon enrichment is expected to be strongly correlated with the carbon content (Schaller et al. 1992; Meynet et al. 1994). In Fig. 7 we compare observed Ne/He and Ne/C versus C/He ratios with theoretical expectations from the Schaller et al. (1992) and Meynet et al. (1994) evolutionary models at solar metallicity for an initial mass of $60M_{\odot}$. We find that observed neon abundances are a factor of two below expectations. Specifically, we derive $\text{Ne}/C = 0.02 \pm 0.01$ in all cases, while $\text{Ne}/C \geq 0.03$ is predicted during this phase of the WC evolution. Error bars shown in the figure account for uncertainties

Table 10. Neon and sulphur abundances derived for the programme stars, using the stellar parameters given in the previous table. In all cases the ionization balance is assumed to consist of He^+ , C^{2+} and O^{2+} . For each star, the first entry refers to the γ_i derived from the (more reliable) integration method, with the second obtained from the analytical expression.

| WR | γ_e | Z | μ | $\gamma_{S^{2+}}$ 10^{-5} | $\gamma_{S^{3+}}$ 10^{-5} | S/He 10^{-5} | γ_{Ne^+} 10^{-4} | $\gamma_{\text{Ne}^{2+}}$ 10^{-4} | Ne/He 10^{-4} |
|-----|------------|-------|-------|--------------------------------|--------------------------------|-------------------|-------------------------------------|--|--------------------|
| 11 | 1.137 | 1.189 | 5.14 | 1.9 | 3.1 | 5.9 | 5.4 | 21.6 | 31.9 |
| | | | | 2.5 | 5.1 | 9.0 | 6.5 | 27.8 | 40.5 |
| 90 | 1.219 | 1.287 | 5.84 | – | – | – | ≤ 4.0 | 22.6 | ≤ 34.0 |
| | | | | – | – | – | ≤ 4.8 | 29.1 | ≤ 43.4 |
| 135 | 1.138 | 1.189 | 5.21 | – | – | – | ≤ 5.9 | 32.0 | ≤ 44.0 |
| | | | | – | – | – | ≤ 7.0 | 41.1 | ≤ 55.8 |
| 146 | 1.083 | 1.117 | 4.70 | – | – | – | ≤ 2.8 | 22.8 | ≤ 28.2 |
| | | | | – | – | – | ≤ 3.3 | 29.5 | ≤ 36.1 |

in distance and (uniform) filling factors, but do not allow for the possibility of a varying volume filling factor between the neon and UV/optical line forming regions, which could be responsible for the discrepant cases.

8 SUMMARY

We have performed quantitative analyses of a small sample of WC5–8 stars, using models that account for line blanketing and clumping. Comparisons between synthetic spectra and de-reddened UV to mid-IR observations are excellent, with few modelling deficiencies identified. Stellar parameters support previous determinations (e.g. Koesterke & Hamann 1995), except that the incorporation of blanketing yields higher stellar luminosities, while clumping indicates lower wind performance numbers, supporting the conclusions of Hillier & Miller (1999) for WR111 (WC5). Future studies will derive properties of WC-type stars, at both earlier (WO) and later (WC9) spectral type, and investigate whether predicted ionizing properties are consistent with nebular observations (e.g. Crowther et al. 1999).

ISO/SWS spectroscopy reveals the presence of neon fine structure transitions, allowing abundance determinations. Using a revised formulation of the BRA88 technique to account for wind clumping, we derive neon abundances of $\text{Ne}/\text{He} = 3\text{--}4 \times 10^{-3}$ by number, seven times higher than the cosmic value adjusted for the H-depleted WC environment, supported by $\text{Ne}/S = 50$ for WR11 from sulphur fine structure lines. The Ne enrichment is a factor of ~ 2 times lower than predictions of current theoretical models. However, differences in volume filling factors between the (high density) UV/optical line formation regions and (low density) mid-IR fine-structure forming regions represent the greatest source of uncertainty in current Ne/He abundance determinations. Nevertheless, Ne/S provides an independent confirmation of the neon enrichment since it is *independent* of outer wind filling factors. Future large ground and space-based telescopes that are optimised for the IR, will allow neon and sulphur line flux measurements and abundance determinations for more distant Wolf-Rayet stars. Of particularly interest are abundances in carbon and oxygen-rich WO stars.

Table 9. Observed mid-IR fine structure line intensities (units of 10^{-12} erg cm $^{-2}$ s $^{-1}$), and adopted atomic parameters, including statistical weights of the upper and lower levels, ω_u and ω_l , transition probability, A_{ul} , and collision strength Ω_{ul} at $T_e=8000$ K. Fluxes are obtained from ISO/SWS observations in all cases, except for literature measurements for WR11, obtained from IRAS/LRS (van der Hucht & Olon 1985) and the UCL spectrometer at the AAT (BRA88).

| Ion | Transition | λ μm | ω_u | ω_l | A_{ul} s^{-1} | Ref | Ω_{ul} 8000K | Ref | WR11 (WC8+O) ISO | WR90 ISO (WC7) | WR135 ISO (WC8) | WR146 ISO (WC5+O) |
|----------|-------------------------------------|----------------------------|------------|------------|-----------------------------|-----|------------------------|-----|---------------------|-------------------|--------------------|----------------------|
| [S IV] | $2P_{3/2}^{\circ}-2P_{1/2}^{\circ}$ | 10.51 | 4 | 2 | 7.70×10^{-3} | a | 8.47 | c | $15 \pm 1^*$ | 19 ± 4 | – | – |
| [Ne II] | $2P_{3/2}^{\circ}-2P_{1/2}^{\circ}$ | 12.81 | 2 | 4 | 8.59×10^{-3} | a | 0.28 | d | 18 ± 1 | ≤ 1 | ≤ 0.5 | ≤ 1 |
| [Ne III] | $3P_{3/2}^{\circ}-3P_{1/2}^{\circ}$ | 15.55 | 3 | 5 | 5.99×10^{-3} | a | 0.76 | e | 82 ± 1 | 6.5 ± 1 | 3.1 ± 0.2 | 9.4 ± 1 |
| [S III] | $3P_{1-1}^{\circ}-3P_{2-2}^{\circ}$ | 18.68 | 5 | 3 | 2.07×10^{-3} | a | 5.30 | b | $< 1.8^*$ | – | – | – |

(a) Naqvi (1951); (b) Galavis et al. (1995); (c) Saraph & Storey (1999); (d) Saraph & Tully (1994); (e) Butler & Zeippen (1994);

(*) [S III-IV] line fluxes are shown prior to correction for the presence of He I and C III stellar features (see text).

ACKNOWLEDGMENTS

This work is based on observations with ISO, an ESA project with instruments funded by ESA Member States (especially the PI countries: France, Germany, the Netherlands and the United Kingdom) with the participation of ISAS and NASA. Theoretical predictions presented here were possible only as a result of the Opacity Project, led by Prof Michael Seaton. Thanks to Dr Tim Harries for observing WR90 on our behalf at the AAT. LD would like to acknowledge financial support from the UCL Perren Fund. PAC acknowledges financial support from a Royal Society University Research Fellowship. DJH gratefully acknowledges support by NASA through grant number NAG5-8211. The Anglo-Australian Telescope, Isaac Newton Telescope and U.K. Infrared Telescope are operated by the Anglo-Australian Observatory, Isaac Newton Group and Joint Astronomy Centre, respectively, on behalf of the Particle Physics and Astronomy Research Council.

REFERENCES

- Abbott D.C., Bieging J.H., Churchwell E. 1981, ApJ 250, 645
 Abbott D.C., Bieging J.H., Churchwell E., Torres A.V, 1986, ApJ, 303, 239
 Barlow M.J., Roche P.F, Aitken D.A., 1988, MNRAS 232, 821 (BRA88)
 Becker S.R., Butler K., 1992, A&A 265, 647
 Becker S.R., Butler K., 1995a, A&A 294, 215
 Becker S.R., Butler K., 1995b, A&A 301, 187
 Butler K., Zeippen C.J., 1994, A&AS 108, 1
 Cardelli J.A., Clayton G.C., Mathis J.S., 1989, ApJ 345, 245
 Chapman J., Leitherer C., Koribalski B., Bouter R., Storey M., 1999, ApJ 518, 890
 Conti P.S., Aschuler W.R., 1971, ApJ 170, 325
 Crowther P.A., Bohannon B., 1997, A&A 317, 532
 Crowther P.A., De Marco O., Barlow M.J., 1998, MNRAS, 296, 367
 Crowther P.A., Pasquali A., De Marco O., Schmutz W., Hillier D.J., de Koter, A., 1999, A&A, 350, 1007
 de Graauw Th., Haser L.N., Beintema D.A., et al. 1996, A&A, 315, L49
 Daly P.N., Beard S.M., 1992, SUN 27 (Rutherford Appleton Laboratory)
 De Marco O., Schmutz W., Crowther P.A. et al. 2000, A&A submitted

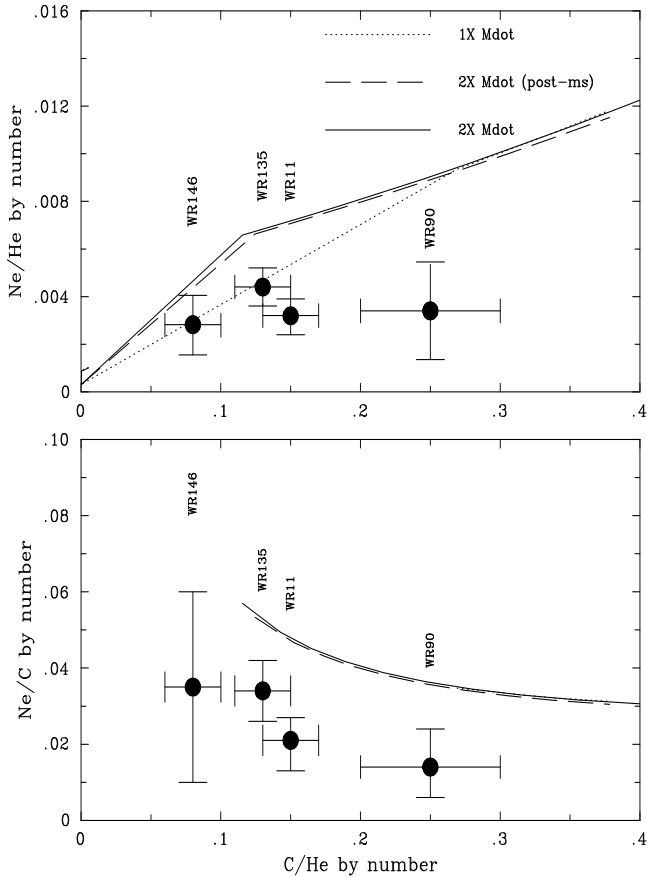


Figure 7. Comparison between Ne/C (bottom) or Ne/He (top) ratios versus measured C/He, also confronted to theoretical expectations from the solar metallicity evolutionary tracks of Schaller et al. (1992) and Meynet et al. (1994) for $60M_{\odot}$. Three tracks are shown: (i) normal mass-loss rates during the entire evolution of the star (dotted); (ii) enhanced ($2\times$) mass-loss during the post main-sequence phase (dashed); (iii) enhanced ($2\times$) mass-loss during the entire stellar evolution (solid). Error bars account for uncertainties in distance and filling factor (see text)

- Dougherty S.M., Williams P.M., van der Hucht K.A., Bode M.F., Davis R.J., 1996, MNRAS, 280, 963
- Dougherty S.M., Williams P.M., Pollacco D.L., 2000, MNRAS in press
- Eenens P.R.J., Williams P.M., Wade R., 1991, MNRAS, 252, 300
- Eenens P.R.J., Williams P.M., 1992, MNRAS, 255, 227
- Fernley J.A., Seaton M.J., Taylor K.T., 1987, J Phys B 20, 6457
- Galavis M.E., Mendoza C., Zeippen C.J., 1995, A&AS 111, 347
- Hillier D.J., 1987, ApJS 68, 947
- Hillier D.J., 1990, A&A 231, 111
- Hillier D.J., 1991, A&A 247, 455
- Hillier D.J., 1996, in: Vreux J.M., Detal A., Fraipont-Caro D., Gosset E., Rauw G. (eds.), Wolf-Rayet stars in the Framework of Stellar Evolution, Proc 33rd Liège Int. Ast. Coll., Université de Liège, p.509
- Hillier D.J., Miller D.L. 1998, ApJ 496, 407
- Hillier D.J., Miller D.L. 1999, ApJ 519, 354
- Howarth I.D., 1983, MNRAS, 203, 301
- Howarth I.D., Phillips, A.P., 1986, MNRAS 222, 809
- Howarth I.D., Schmutz W., 1992, A&A 261, 503
- Howarth I.D., Murray J., Mills D., Berry D.S., 1998 SUN 50.21, (Rutherford Appleton Laboratory)
- van der Hucht K.A., Olnon F.M., 1985, A&A 149, 17
- van der Hucht K.A., Conti P.S., Lundström I., Stenholm B., 1981, Space Sci. Rev. 28, 227
- van der Hucht K.A., Hidayat B., Admiranto, A.G., Supelli K.R., Doom C., A&A 1988, 199, 217
- van der Hucht, K.A., Morris P.W., Williams P.M., et al. 1996, A&A 315, L193
- van der Hucht, K.A., Schrijver H., Stenholm, B., et al. 1997, New Astronomy, 2, 245
- de Jager C., Nieuwenhuijzen H., van der Hucht K.A., 1988, A&AS 72, 259
- Kessler M., Steinz J.A., Anderegg M.E., et al., 1996, A&A, 315, L27
- Koesterke L., Hamann W.-R., 1995, A&A, 299, 503
- Kurucz R.L., 1991, in: Philip A.G.D., Uppgren A.R., Janes K.A. (eds.), Precision Photometry: Astrophysics of the Galaxy, L. Davis Press, Schenectady, p.27
- Langer N., 1989, A&A 220, 135
- Leitherer C. Champan, J.M., Koribalski B., 1997 ApJ 481, 898
- Lepine S., Moffat A.F.J., 1999, ApJ 514, 909
- Lundström I., Stenholm B., 1984, A&AS 58, 163
- Luo D., Pradhan A.K., Saraph H.E., Storey P.J., Yu Yan., 1989, J Phys B., 22, 389
- Luo D., Pradhan A.K., 1989, J Phys B., 22, 3377
- Massey P., 1984, ApJ 281, 789
- Meynet G., Maeder A., Schaller G., Schaerer D., Charbonnel C., 1994, A&AS 103, 97
- Moffat A.F.J., Drissen L., Lamontagne R., Robert C., 1988, ApJ 334, 1038
- Moffat A.F.J. 1999, in Wolf-Rayet Phenomena in Massive Stars and Starburst Galaxies, eds. K.A. van der Hucht, G. Koenigsberger & P.R.J. Eenens, Proc. IAU Symp. No. 193 (San Francisco: ASP), 278
- Morris P.W., Brownsberger K.R., Conti P.S., Massey P., Vacca W.D., 1993, ApJ 412, 324
- Morris P.W., van der Hucht, K.A., Willis A.J., Williams P.M., 1998, Ap&SS 255, 157
- Morris P.W., van der Hucht, K.A., Crowther P.A., Dessart L., Willis A.J., Williams P.M., 2000, A&A 353, 624
- Morris P.W., van der Hucht, K.A., et al. 2000, A&A in prep.
- Naqvi A.M., 1951, Thesis, Harvard
- Niemela V., Shara M.M., Wallace D.J., Zurek D.R., Moffat A.F.J., 1998 AJ 115, 2047
- Nussbaumer H., Storey P.J., 1983, A&A 126, 75
- Nussbaumer H., Storey P.J., 1984, A&AS 56, 293
- Peach G., Saraph H.E., Seaton M.J., 1988 J Phys B. 21, 3669
- Prinja R.K., Barlow M.J., Howarth I.D., 1990, ApJ 361, 607
- St Louis N., 1990, PhD thesis, University of London
- St-Louis N., Willis A.J., Stevens I.R., 1993, ApJ 415, 298
- Saraph H.E., Tully, J.A. 1994, A&AS 107, 29
- Saraph H.E., Storey P.J., 1999, A&AS 134, 369
- Schaeidt S., Morris, P.W., Salama, A., et al. 1996, A&A, 315, L60
- Schaerer D., Maeder A., 1992, A&A 263, 129
- Schaerer D., Schmutz W., Grenon M., 1997 ApJ 484, L153
- Schaller G., Schaerer D., Meynet G., Maeder, A., 1992, A&AS 96, 269
- Schmutz W. 1997, A&A 321, 268
- Schmutz W., Vacca W.D., 1991, A&AS 89, 259
- Seaton M.J., 1987, J. Phys B., 20, 6363
- Seaton M.J., 1995, The Opacity Project Volume 1, Institute of Physics Publishing, Bristol.
- Shortridge K., Meyerdieks H., Currie M., et al. 1999, SUN 86.17 (Rutherford Appleton Laboratory)
- Smith L.F., 1968, MNRAS 140, 409
- Smith L.F., Shara, M.M., Moffat, A.F.J., 1990, ApJ 358, 229
- Steenman H., Thé P.S., 1989, Ap&SS 159, 189
- Steenman H., Thé P.S., 1991, Ap&SS 184, 9
- Stevens I.R. Corcoran M.F., Willis A.J. et al. ,1996, MNRAS, 283, 589
- Torres-Dodgen A.V., Massey P., 1988, AJ 96, 1076
- Torres-Dodgen A.V., Carroll M., Tapia M., 1991, MNRAS 249, 1
- Tully J.A., Seaton M.J., Berrington K.A., 1990, J Phys B 23, 3811
- Wiese W.L., Smith M.W., Glennon B.M., 1966, Atomic Transition Probabilities, Volume I Hydrogen Through Neon, NSRDS-NDS 4.
- Willis A.J., van der Hucht K.A., Garmany C.D., Conti P.S., 1986, A&AS, 63, 417
- Willis A.J., Dessart L., Crowther P.A., et al. 1997, MNRAS 290, 371 (Paper I)
- Wright A.E., Barlow M.J., 1975, MNRAS, 170, 41 J Phys B 22, 389
- Yu Yan, Taylor K.T., Seaton M.J., 1987, Phys B. 20, 6399
- Yu Yan, Seaton M.J., 1987, Phys B. 20, 6409